

Article

Protective Properties of Calcareous Deposit Layer for Cathodically Polarized AH36 Steel in Natural Seawater

Quoc Quang Nong ^{*}, Van Kien Dong, Van Trieu Nguyen, Van Chi Nguyen , Hong Quan Le  and Nhat Linh Cao

Coastal Branch, Joint Vietnam-Russia Tropical Science and Technology Research Center, 30 Nguyen Thien Thuat, Nha Trang 650000, Vietnam

^{*} Correspondence: quangnq@vrtc.org.vn

Abstract: A calcareous deposit is a by-product of the cathodic polarization in seawater environments. This study presents the results of evaluating the anticorrosion and anti-macro-biofouling effectiveness of a calcareous deposit layer on the surface of the cathodically polarized AH36 structural steel in tropical seawater. The polarization is induced with initial current densities at which the calcareous deposit layer formed with both aragonite and brucite for 12 months continuously. The protective properties of the layer were compared with those of the passive layer from corrosion products under the same environmental conditions. The macro-biofouling in the tropical seawater is observed in the closed and open surfaces of the steel. The comparison of the anticorrosion property shows that, to some degree, the calcareous deposit layer contributes to surface passivation, as in the case of the corrosion product layer. In addition, the composition of the brucite and aragonite in the calcareous layer in the study plays a role as a macro-biofouling growth-limiting factor.

Keywords: calcareous deposit layer; marine corrosion; AH36 structural steel; macro-biofouling; tropical seawater



Citation: Nong, Q.Q.; Dong, V.K.; Nguyen, V.T.; Nguyen, V.C.; Le, H.Q.; Cao, N.L. Protective Properties of Calcareous Deposit Layer for Cathodically Polarized AH36 Steel in Natural Seawater. *Coatings* **2024**, *14*, 644. <https://doi.org/10.3390/coatings14050644>

Academic Editor: Yanxin Qiao

Received: 26 April 2024

Revised: 13 May 2024

Accepted: 13 May 2024

Published: 19 May 2024



Copyright: © 2024 by the authors. Licensee MDPI, Basel, Switzerland. This article is an open access article distributed under the terms and conditions of the Creative Commons Attribution (CC BY) license (<https://creativecommons.org/licenses/by/4.0/>).

1. Introduction

AH36 steel has been widely used as the substrate material for the submerged static structures in the marine environment, where the substrates are affected by both corrosion and biofouling. One of the most common corrosion protection techniques for such structures is cathodic polarization using an impressed current. The advantage of this technique is that it can be applied to large and structurally complex projects, especially structures submerged in seawater. Until the present time, the effectiveness of the technique has been widely acknowledged [1–5]. The research carried out on this technical platform also extends towards improving the polarization efficiency or optimizing the energy use, as well as exploiting possible results from the application of the protection mechanisms above [6–8].

In the process of polarization, the protected objects play a role as cathodes. The by-product that appears from the beginning of the polarization process on the surface of the protected objects is a calcareous deposit layer of some precipitates of calcium and magnesium ions from natural seawater, in which the ions exist in abundant quantities and move freely among the electrodes [9–14]. The mechanism of the precipitation is the increasing pH locally on the surfaces of the cathode from the oxidation–reduction reactions, which is the favorable condition of the series of reactions, with the last products containing CaCO_3 and $\text{Mg}(\text{OH})_2$ [15–18].

The formation of the calcareous layer is influenced by environmental factors, including the environmental temperature, salinity, pH, dissolved oxygen concentration, calcium and magnesium ions concentration, etc., and microbial factors, with the result that the characteristic components can only be formed in the natural environment. However, to facilitate the monitoring and processing evaluation, studies on this phenomenon are conducted in the laboratory with both natural and artificial seawater [19,20]. The formation process of the

calcareous layer, as well as the current density dependent on the deposition, were widely published through the laboratory studies. The published analytical results show that the main component of the calcareous deposit layer is brucite. In addition, depending on the current density maintained between the cathode and anode, the precipitation products of the calcium ions can be calcite, aragonite, or vaterite [21–26].

In this study, the calcareous deposit layer was formed on the surface of AH36 structural steel with cathodic polarization in natural seawater. The bare AH36 steel was exposed parallelly in the same environmental conditions, and the process of the corrosion of the AH36 structural steel happened such that the comparison of the anticorrosion properties between the layer of the calcareous deposit and the layer from the corrosion products was induced. The conditions for the deposition of the precipitates were created in which the composition of the resulting precipitates was chosen to favor a durable coating and was recommended for the investigation by previous research groups in a laboratory setting [15,21]. This means that the current density between the electrodes is maintained at a certain range consistent with the previous publications. With the resulting surfaces of the cathodically polarized AH36 steel, we tried to characterize the calcareous layers from the precipitates of CaCO_3 and $\text{Mg}(\text{OH})_2$ by the SEM and XRD techniques, and the electrochemical performance of the surfaces of the AH36 steel was then studied. In addition, the macro-biofouling on the layer was evaluated through 12 months of polarization.

2. Materials and Methods

2.1. Materials

The AH36 structural steel plate used for cathode material was cut into the size of $150 \text{ mm} \times 100 \text{ mm} \times 3 \text{ mm}$ with the compositions in wt% as shown in [27]. Before immersion and polarizing in seawater as a cathode, the plates were polished with SiC paper and cleaned in acetone. The cleaned plates were then immersed in solution consisting of 0.35 wt% hexamethylenetetramine and 0.5 M HCl for 30 min and then cleaned with distilled water and dried at room temperature for 8 h.

For the purpose of analyzing the layers formed on the surface of the samples through potentiostat Metrohm PGSTAT 204N Autolab electrochemical device (Metrohm Autolab BV, Utrecht, The Netherlands), a glass cut from the PVC tube with an inner diameter of 34 mm was fixed on the surface of the AH36 steel plate by the 2-component epoxy glue. The working electrode from AH36 steel was then determined as a definite zone limited by a circle and joined in a three-electrode cell with the platinum auxiliary electrode and Ag/AgCl reference electrode.

2.2. Polarizing Method

A power supply is used to polarize the AH36 steel plates in natural seawater at Dam Bay Marine Climatic Testing Station ($12^\circ 11' 49.8'' \text{ N}$, $109^\circ 17' 26.2'' \text{ E}$), Nha Trang, Khanh Hoa. AH36 steel plate is cathodically polarized by a DC power source with initially stabilized current (initial current density is fixed). The potential is constant through the process, and the downward trend of the current induced through cathode was monitored. Bias voltage and current values are recorded by dataloggers SD910 and SD 900 (EXTECH) 3 real-time channels.

The cathodic protection potential between the electrodes is maintained in accordance with BS EN 12495:2000 and DNV-RB-B401, in which the protection potential ranges from -1.1 to -0.8 V vs. Ag/AgCl.

2.3. Sampling Methods and Analysis Techniques

After being polarized in natural seawater, the test samples were dried using a UN260 oven (Memmert GmbH, Schwabach, Germany) at a temperature of 80°C for 4 h. The mass of the test sample before and after the polarization was determined using the technical scale PA 4102, OHAUS.

The surface morphology of scale deposits on AH36 steel substrate was photographed and analyzed under a scanning electron microscope (SEM, Hitachi, S-4800) associated with energy dispersive X-ray spectroscopy. Calcareous deposit components were analyzed through X-ray diffraction spectroscopy (XRD, PANalytical, X'Pert-PRO MPD, Almelo, The Netherlands) using Cu-K emission source.

3. Results and Discussion

3.1. Characteristics of the Calcareous Deposit

After cathodic polarization for 4 h with a current density of 3 A/m^2 , the filled steel surface by the calcareous deposit was analyzed. The SEM image shows the formation of the deposit at the beginning of the polarization process. The EDS spectrum shows the apparent trace element peaks of magnesium, oxygen, and calcium, especially magnesium in the initial period of polarization (Figure 1). The magnesium-rich layer of the calcareous deposit revealed the priority in the precipitation of $\text{Mg}(\text{OH})_2$ in the beginning of the deposition process. The polarization is maintained for months with a range of initial current density from 2 to 4 A/m^2 . After 6 months, the polarization forms a thick layer of a compound of calcium and magnesium; the crystal structure is found under the XRD patterns presented in Figure 2.

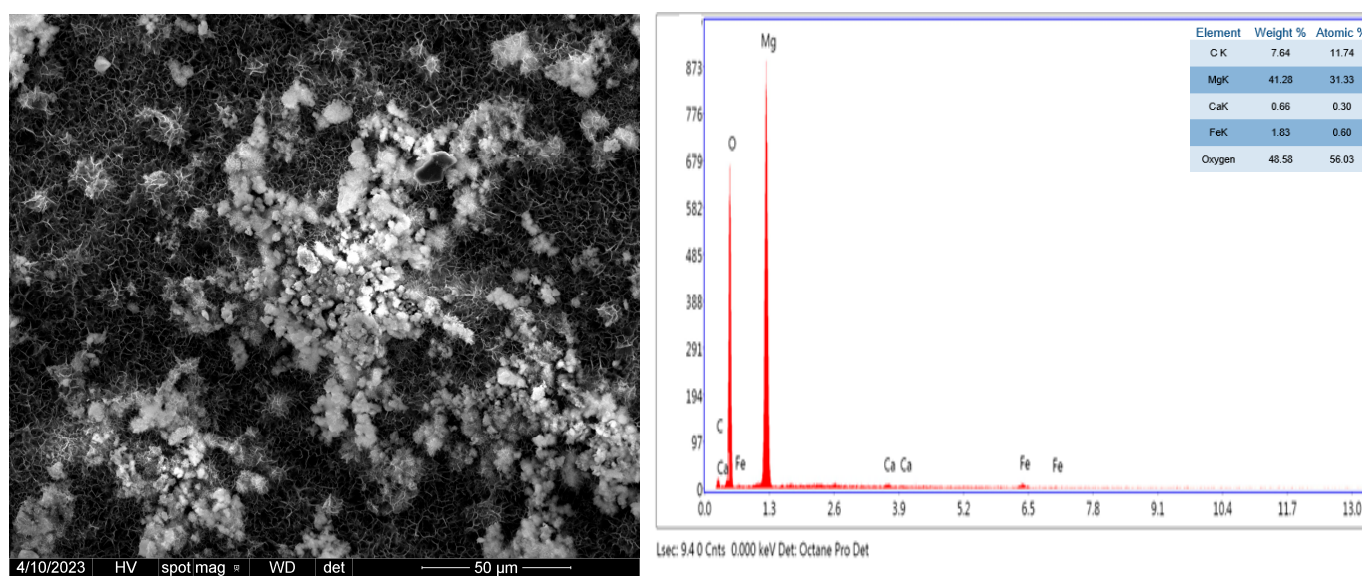


Figure 1. The SEM image and the EDS spectrum of the calcareous deposit layer formed on the surface of the cathode for the first 4 h with current density of 3 A/m^2 .

From the XRD patterns, the aragonite and brucite are identified with PDF numbers 0-003-0425 and 01-073-8391 accordingly. The relative proportions of the phases of aragonite and brucite using the X-ray diffraction (XRD) patterns are typically 32:68 and 16.8:83.2 in the samples with current densities of 3 A/m^2 and 2 A/m^2 . The difference in the aragonite and brucite composition ratios can be explained by the higher precipitation rate at higher current densities, where, after favoring the same amount of magnesium ion precipitation, the precipitate of calcium will continue above the magnesium precipitate layer. No peaks regarding the other compounds, for example calcite or vaterite, were found. The compound from aragonite and brucite was found to be the most adhesive to the substrate AH36 steel, and the washing phenomena in seawater environments at different flow rates are limited, and the calcareous layer is suitable for evaluating the protective property, as well as biofouling [15,21].

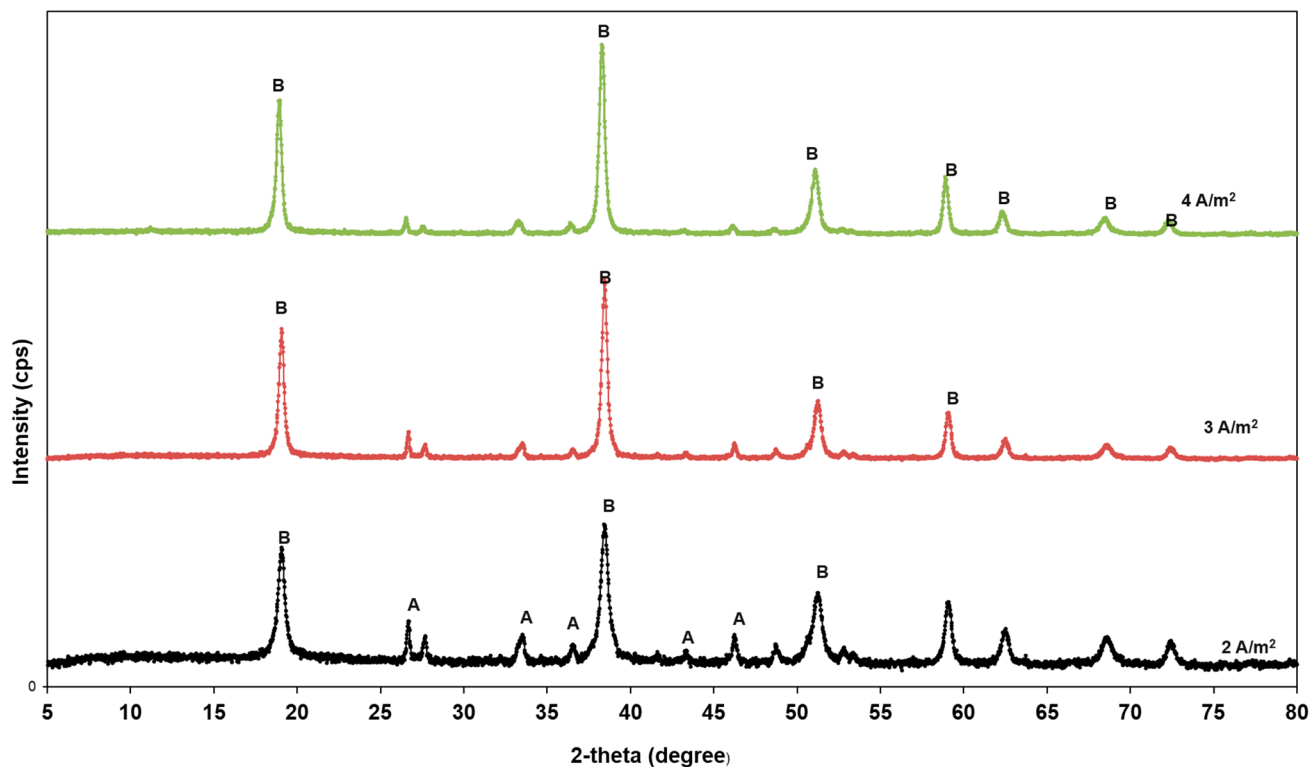


Figure 2. XRD patterns collected on the surface of polarized AH36 structural steel at different current densities with diffraction peaks of aragonite (A) and brucite (B).

3.2. Electrochemical Performance

3.2.1. Polarization Curves

The AH36 steel plates were polarized in the natural seawater with current densities of 3 A/m^2 . After a definite period of time, the area inside the PVC tube was observed to be deposited with a calcareous layer. Figure 3 presents the Tafel polarization curves of the AH36 bare steel and AH36 cathode in natural seawater for 1, 5, 9, and 12 months. After 9 months, the surface of the AH36 steel was covered under a passive film of corrosion products and biofouling [27–29]; the surface of the polarized AH36 steel was filled with white precipitates. The shift in the curves towards more positive potentials for the AH36 steel samples immersed in seawater indicates that passivation is established for the corroded AH36 steel containing corrosion products on the surface. However, the shift in the curves in the opposite direction for the polarized steel from the fifth month onwards may be related to the altered porous nature of the surface calcareous layer, while the aragonite precipitated more. In the case of an increased aragonite accumulation, the calcareous layer must still facilitate the maintenance of charge exchange, so it is not entirely correct to say that further accumulation of aragonite makes the calcareous layer more condensed. The presence of aragonite at this stage is proven by the XRD analysis results presented above. From the Tafel extrapolation results in Table 1, the changes in the corrosion potential and corrosion current density are shown in Figure 4, in which the changes in these quantities are presented during the same test period for the immersed AH36 steel and polarized AH36 steel in natural seawater. There is a clear difference at the beginning of the polarization and immersion in seawater for bare steel AH36; however, near the end of the testing period (1 year), the values of the corrosion current density and potential corrosion in both cases were nearly equivalent. This proves that the steel surface in the two test conditions is passivated to a similar extent.

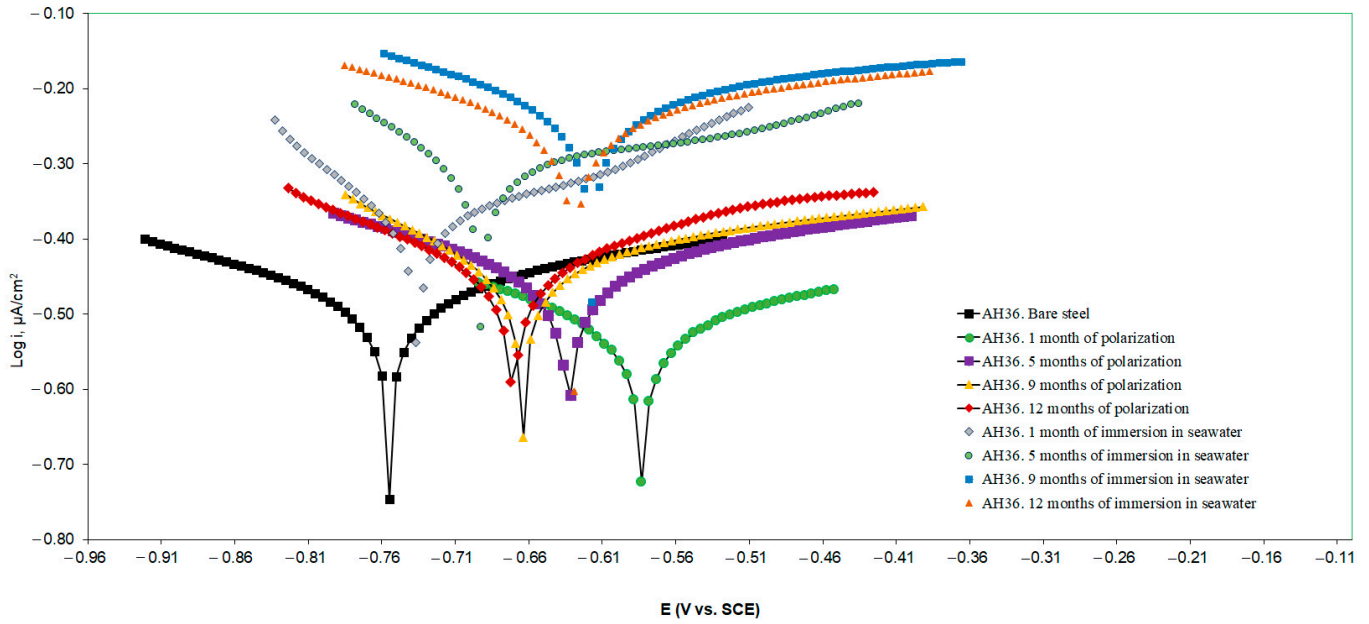
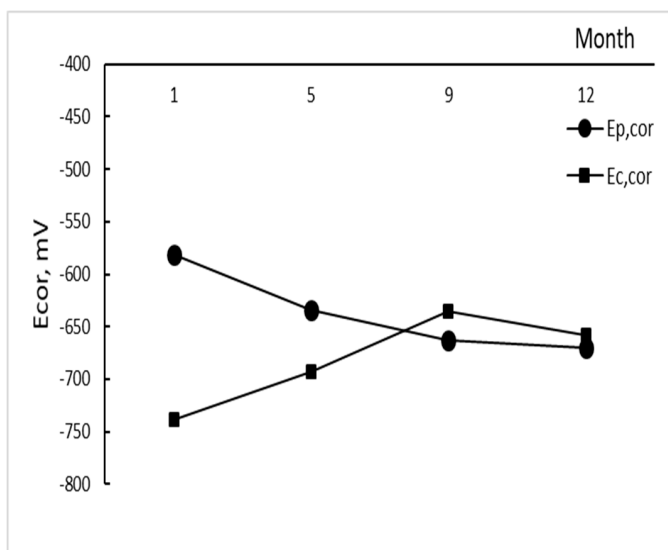


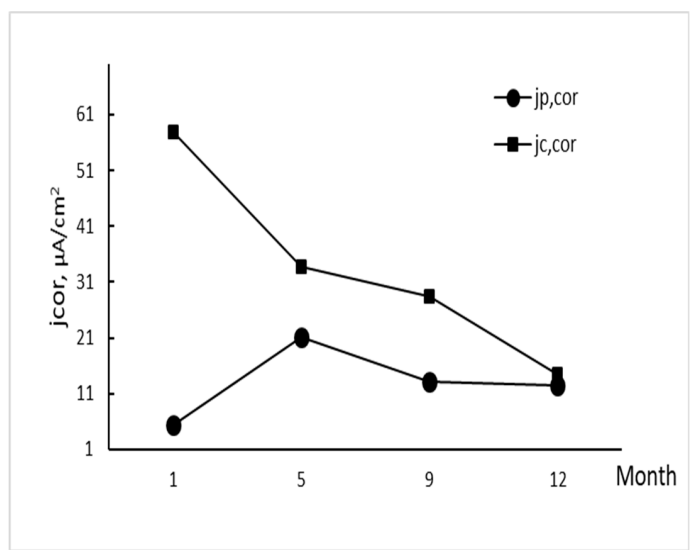
Figure 3. Polarization curve shifts of AH36 steel and cathodically polarized AH36 steel in natural seawater.

Table 1. Electrochemical parameters extrapolated from the polarization curves of the AH36 steel cathode samples and unprotected AH36 steel samples with initial current density 3 A/m².

Parameters from Extrapolation	AH36 Steel Cathode Samples/Unprotected AH36 Steel Samples				AH36 Bare Steel
	for 1 Month	for 5 Months	for 9 Months	for 12 Months	
Corrosion potential (mV)	−581/−738	−634/−693	−663/−635	−670/−658	−736
Corrosion current density (µA/cm ²)	5.4/57.9	21.1/33.8	13.1/28.5	12.5/14.5	58.5
Polarization resistor (Ω)	1991/65.7	496/188	372/65.6	373/76	65.6
Anode slope β _a (mV/dec)	347/107	355/148	149/109	180/359	109
Cathode slope β _c (mV/dec)	638/306	565/1311	317/303	213/657	303



(a)



(b)

Figure 4. Changing trends of corrosion potential (a) and corrosion current density (b) for AH36 bare steel and AH36 polarized steel in natural seawater over time.

Figure 5 shows the round areas on the two kinds of samples in the electrochemical analysis after 5 months. Corrosion products exist on the surface of the AH36 steel, causing the passivation of the surface. The surface selected for the investigation with the electrochemical equipment in this case does not contain macro-biofouling that would interfere with the investigated parameters. In the case of polarized AH36 steel, the surface containing white precipitates also showed no signs of biofouling. The parameters from the Tafel extrapolation are shown in Table 1 with the exposing period. At the beginning of the polarization, the corrosion current density from the cathode is significantly smaller than that from the bare steel, while the corrosion potentials change in the range of 150 mV, so the calcareous deposit layer on the cathodes has a role regarding the inhibition of the corrosion process in natural seawater to some degree.

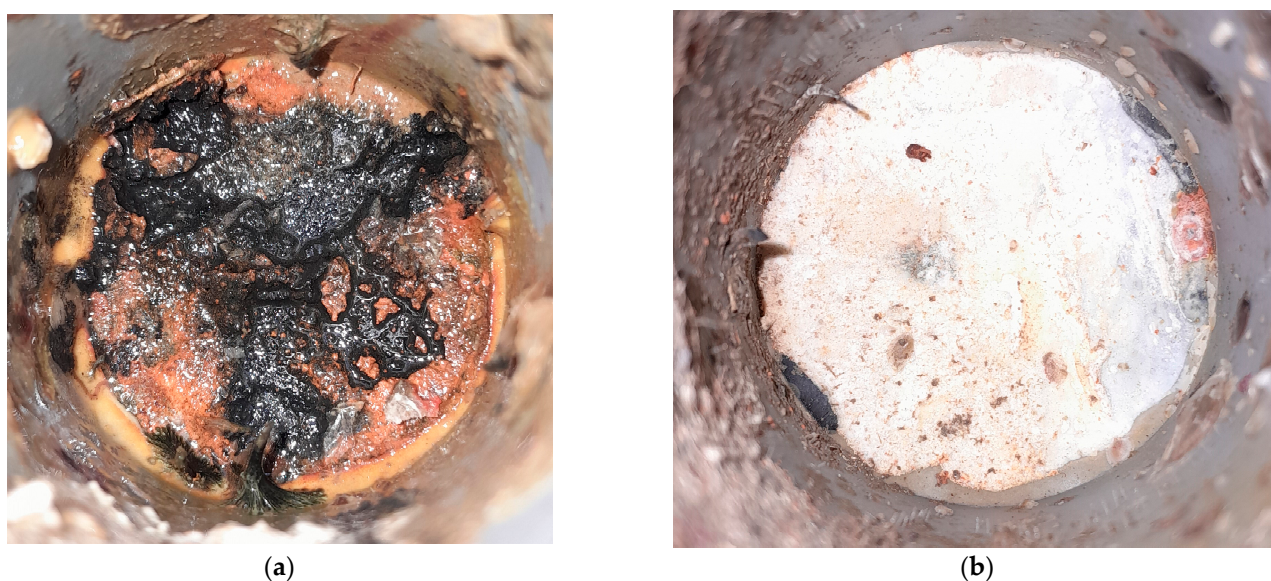


Figure 5. Round areas for electrochemical analyses on (a) the surfaces of AH36 steel and (b) cathodically polarized AH36 steel with natural seawater.

3.2.2. Electrochemical Impedance

The EIS measurements were performed in situ after the AH36 steel was polarized continually. This means that the AH36 steel will be examined with different surfaces containing corrosion products and containing calcareous deposits. The Nyquist diagrams of the AH36 steel cathode are shown in Figure 6 with frequency covers ranging from 10^{-2} Hz to 10^5 Hz. For the AH36 bare steel, the equivalent circuit can be described as the series of electrolyte resistance R_e and a double-layer element in which the charge transfer resistance R_{Ct} is in parallel with the double-layer capacitance C_{dl} . The equivalent circuit of impedance for the polarized steel can be illustrated using the five-element model [26,30] in Figure 7. In this five-element model, the double-layer element, consisting of double-layer capacitance CPE_1 in parallel with the charge transfer resistance R_{Ct} , is in series with the electrolyte resistance R_f in the thin pore. The above series connects parallelly to a capacitive element CPE_2 to model the calcareous layer with a dielectric nature. The last element, electrolyte resistance R_e , is connected in series with the calcareous layer modeling element. The fitting results are shown in Table 2. The value of R_f (the finite conductivity of the electrolyte in the thin pores) is increased and reaches stability. R_e (electrolyte resistance) and R_{Ct} (charge transfer resistance) increased with the time of polarization. The value of R_{Ct} reached stability after 9 months, showing that the calcareous deposit layer is more stable over time. This may be attributed to the fact that the brucite- $Mg(OH)_2$ formed initially and then a layer was added with more aragonite - $CaCO_3$, through which the calcareous layer is more stable [19].

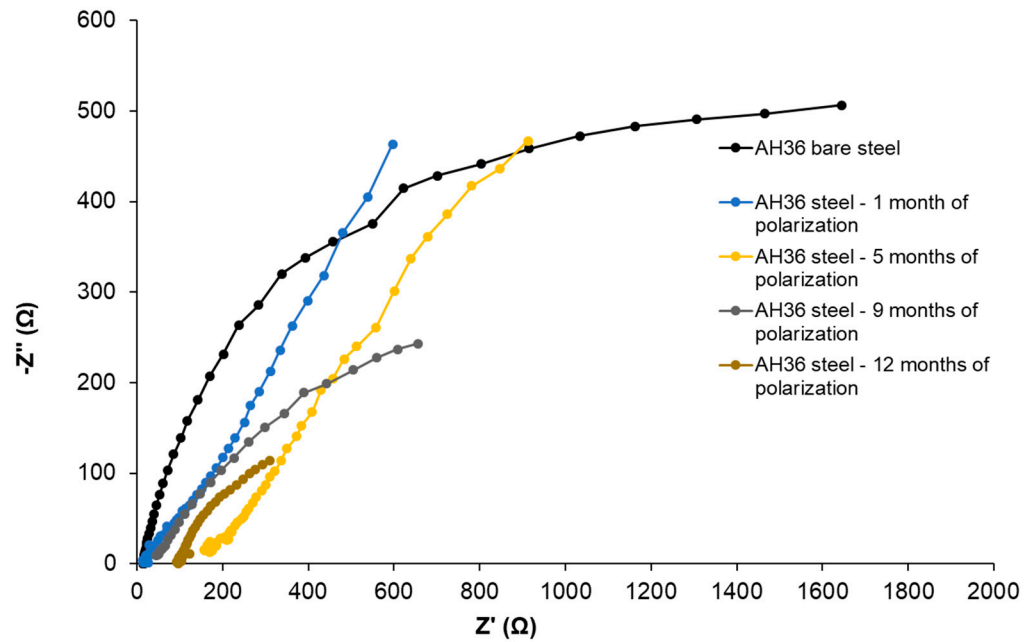


Figure 6. Nyquist diagrams of EIS measurements on samples with various time periods of polarization.

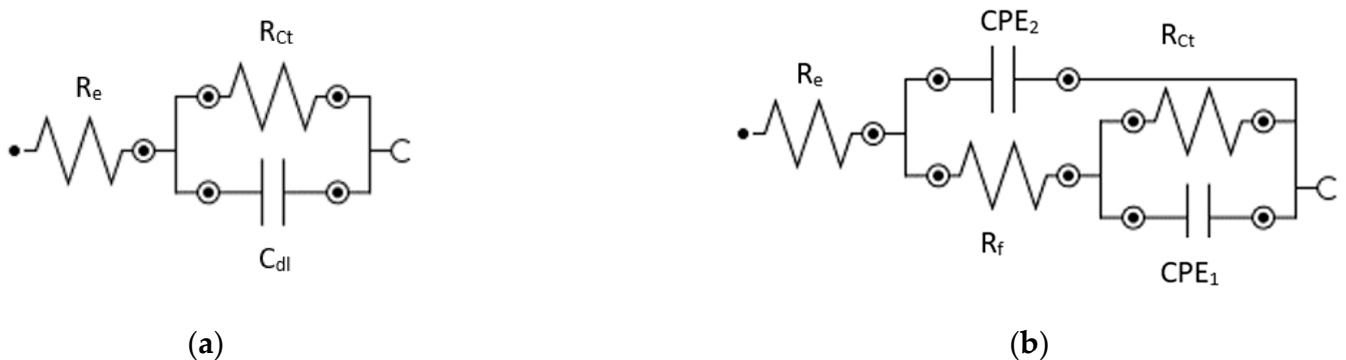


Figure 7. Equivalent circuit diagrams: (a) AH36 bare steel; (b) AH36 steel with substrate covered by calcareous deposits.

Table 2. The EIS fitting results with various periods of polarization for AH36 steel.

Parameters	AH36 Bare Steel	AH36-1	AH36-5	AH36-9	AH36-12
R_e ($\Omega \cdot \text{cm}^2$)	1.3	1.93	6.08	15.86	32.2
R_{ct} ($\Omega \cdot \text{cm}^2$)	65.6	50.23	45.94	70.39	70.6
R_f ($\Omega \cdot \text{cm}^2$)	-	9.53	15.31	13.33	13.88
CPE_1 * ($\mu\text{F} \cdot \text{cm}^{-2}$)	-	53,463	29,137	45,294	14,250
CPE_2 * ($\mu\text{F} \cdot \text{cm}^{-2}$)	-	1180	1652	481	726
C_{dl} ($\mu\text{F} \cdot \text{cm}^{-2}$)	1159	-	-	-	-

* CPE1: the model of double-layer capacitance; CPE2: the model of the calcareous deposit capacitance. C_{dl} : double-layer capacitance on the surface of bare AH36 steel.

3.3. The Macro-biofouling

The macro-biofouling was monitored through two kinds of surfaces: the surface surrounded inside the PVC tube, which is used for electrochemical analysis, and the open surface of the whole $150 \times 100 \times 3$ mm of the cathode. The surfaces are filled with precipitates of magnesium ions at the beginning and then precipitates of calcium ions

accumulated on the surfaces containing brucite. The composition of this compound, as examined by the XRD technique, is mainly brucite and aragonite. The properties of the surface make the precipitates non-uniformly distributed [31]. In general, our research group found no clear evidence of macro-biofouling on the monitored surface, as shown in Figure 8.

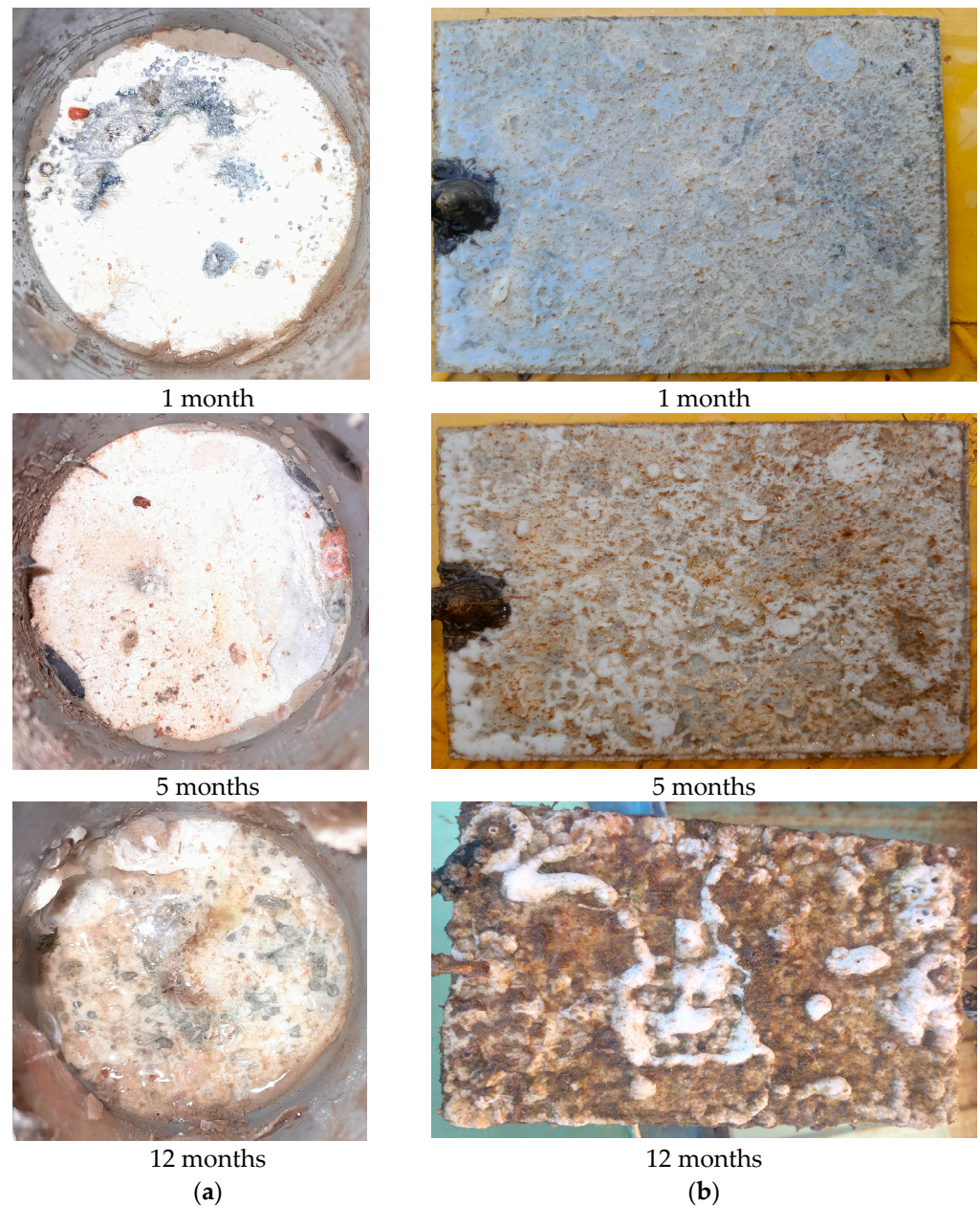


Figure 8. Two kinds of surfaces exposed for macro-biofouling experiment: (a) surface limited by PVC tube; (b) open surface of cathode.

Not only in closed surfaces but also in open ones, the development of the calcareous deposit invaded the appearance of the macro-biofouling. If the bacterial activity appeared to change the preferential formation of the calcareous deposits and impeded the formation of the aragonite and brucite, then the composition of the brucite and aragonite formed within a certain current density range around 3 A/m^2 in this study, playing an essential role regarding the macro-biofouling growth-limiting factor on the surface.

4. Conclusions

Via electrochemical performance comparison, the calcareous deposit layer formed through the process of cathodic polarization is found to have barrier properties similar to the corrosion product layer on the surface of the AH36 steel in natural seawater. In addition, the presence of a calcareous deposit layer containing both aragonite and brucite limits the macro-biofouling development on the surface when the polarized AH36 steel is immersed in tropical seawater.

Author Contributions: Conceptualization, Q.Q.N.; methodology, N.L.C., V.C.N., and Q.Q.N.; investigation, V.T.N. and V.K.D.; formal analysis, H.Q.L.; data curation, Q.Q.N. and N.L.C.; writing—original draft preparation, Q.Q.N.; writing—review and editing, N.L.C. and V.C.N. All authors have read and agreed to the published version of the manuscript.

Funding: This section is devoted to acknowledging the support through the research funding from The Joint Vietnam–Russia Tropical Science and Technology Research Center under Grant number 1502/QĐ-TTNDVN 20.5.2022 of The Ecolan T-1.2 Project 4th.

Institutional Review Board Statement: Not applicable.

Informed Consent Statement: Not applicable.

Data Availability Statement: The data presented in this study are available in the article.

Acknowledgments: We would like to thank Filichev N. L. for his encouragement and visits throughout the research process. Thank you Mikurov D. S. for always being by our side on field trips and always offering to help in the most difficult times. Thank you to the Coastal Branch of the Joint Vietnam-Russia Tropical Science and Technology Research Center, especially the Tropical Durability Department, for always providing full support with equipment and laboratories for the research team to work smoothly.

Conflicts of Interest: The authors declare no conflicts of interest.

References

1. Vedaprakash, L.; Dineshram, R.; Ratnam, K.; Lakshmi, K.; Jayaraj, K.; Mahesh Babu, S.; Venkatesan, R.; Shanmugam, A. Experimental studies on the effect of different metallic substrates on marine biofouling. *Colloids Surf. B Biointerfaces* **2013**, *106*, 1–10. [[CrossRef](#)]
2. Crupi, V.; Guglielmino, E.; Maestro, M.; Marino, A. Fatigue analysis of butt welded AH36 steel joints: Thermographic method and design S-N curve. *Mar. Struct.* **2009**, *22*, 373–386. [[CrossRef](#)]
3. Lu, Y.; Ding, Y.; Wang, M.; Yang, L.; Wang, Y. An environmentally Friendly Laser Cleaning Method to Remove Oceanic Micro-Biofoulings from AH36 Steel Substrate and Corrosion Protection. *J. Clean. Prod.* **2021**, *314*, 127961–127972. [[CrossRef](#)]
4. Vulkelic, G.; Vizingin, G.; Ivosevic, S.; Bozic, Z. Analysis of prolonged marine exposure on properties of AH36 steel. *Eng. Fail. Anal.* **2022**, *135*, 106132. [[CrossRef](#)]
5. Wang, L.; Li, H.; Huang, Y.; Wang, K.; Zhou, M. Effect of Preheating on Martensitic Transformation in the Laser Beam Welded AH36 Steel Joint: A Numerical Study. *Metals* **2022**, *12*, 127. [[CrossRef](#)]
6. Pratikno, H.; Titah, H.S.; Handayanu Mahardhika, G.R. Impressed Current Anti Fouling (ICAF) to Reduce Population of *Chlorella Vulgaris* Cause Bio Corrosion on AH36 Steel in Marine Environment. *E3S Web Conf.* **2019**, *125*, 06001. [[CrossRef](#)]
7. Michopoulos, J.G.; Iliopoulos, A.P.; Steuben, J.C.; DeGiorgi, V. Towards an Analytical, Computational and Experimental Framework for Predicting Aging of Cathodic Surfaces. In Proceedings of the ASME 2017 International Design Engineering Technical Conferences and Computers and Information in Engineering Conference, Cleveland, OH, USA, 6–9 August 2017; Volume 1. [[CrossRef](#)]
8. Touzain, S.; Le Thu, Q.; Bonnet, G. Evaluation of thick organic coatings degradation in seawater using cathodic protection and thermally accelerated test. *Prog. Org. Coat.* **2005**, *52*, 311–319. [[CrossRef](#)]
9. Li, X.W.; Du, S.M.; Ma, C.H.; Shi, T.; Qi, W.; Yang, H.J. Nano-SiO₂ based anti-corrosion superhydrophobic coating on Al alloy with me-mechanical stability, anti-pollution and self-cleaning properties. *Ceram. Int.* **2024**, *50*, 9469–9478. [[CrossRef](#)]
10. Pedferri, P. Evans Diagrams. In *Corrosion Science and Engineering. Engineering Materials*; Springer, Springer Nature Switzerland: Cham, Switzerland, 2018; 737p.
11. Googan, C. The cathodic protection potential criteria: Evaluation of the evidence. *Mater. Corros.* **2020**, *72*, 446–464. [[CrossRef](#)]
12. Carré, C.; Zanibellato, A.; Jeannin, M.; Sabot, R.; Gunkel-Grillon, P.; Serres, A. Electrochemical calcareous deposition in seawater. A review. *Environ. Chem. Lett.* **2020**, *18*, 1193–1208. [[CrossRef](#)]
13. Chen, T.; Neville, A.; Yuan, M. Calcium carbonate scale formation –assessing the initial stages of precipitation and deposition. *J. Pet. Sci. Eng.* **2005**, *46*, 185–194. [[CrossRef](#)]

14. Tlili, M.M.; Benamor, M.; Gabrielli, C.; Perrot, H.; Tribollet, B. Influence of the interfacial pH on electrochemical CaCO₃ precipitation. *J. Electrochem Soc.* **2003**, *150*, C765. [[CrossRef](#)]
15. Loto, C. Calcareous Deposits and Effects on Steels Surfaces in Seawater—A Review and Experimental Study. *Orient. J. Chem.* **2018**, *34*, 2332–2341. [[CrossRef](#)]
16. Barchiche, C.; Deslouis, C.; Festy, D.; Gil, O.; Refait, P.; Touzain, S.; Tribollet, B. Characterization of calcareous deposits in artificial seawater by impedance techniques: III. Deposit of CaCO₃ in the presence of Mg(II). *Electrochim. Acta* **2003**, *48*, 1645–1654. [[CrossRef](#)]
17. Barchiche, C.; Deslouis, C.; Gil, O.; Refait, P.; Tribollet, B. Characterisation of calcareous deposits by electrochemical methods: Role of sulphates, calcium concentration and temperature. *Electrochim. Acta* **2004**, *49*, 2833–2839. [[CrossRef](#)]
18. Stumm, W.; Morgan, J. *Aquatic Chemistry. Chemical Equilibria and Rates in Natural Water*; J. Wiley and Sons. Inc.: Hoboken, NJ, USA, 1996.
19. Carré, C.; Gunkel-Grillon, P.; Serres, A.; Jeannin, M.; Sabot, R.; Quiniou, T. Laboratory and in situ investigations for trapping Pb and Ni with an unusual electrochemical device, the calcareous deposit in seawater. *Sci. Rep.* **2019**, *9*, 3–10. [[CrossRef](#)]
20. Eashwar, M.; Subramanian, G.; Palanichamy, S.; Rajagopal, G.; Madhu, S.; Kamaraj, P. Cathodic behaviour of stainless steel in coastal Indian seawater: Calcareous deposits overwhelm biofilms. *Biofouling* **2009**, *25*, 191–201. [[CrossRef](#)]
21. Park, J.M.; Lee, M.H.; Lee, S.H. Characteristics and Crystal Structure of Calcareous Deposit Films Formed by Electrodeposition Process in Artificial and Natural Seawater. *Coatings* **2021**, *11*, 1–12. [[CrossRef](#)]
22. Nguyen, D.D.; Gascoin, S.; Zanibellato, A.; Da Silva, C.; Lemoine, M.; Riffault, B.; Sabot, R.; Jeannin, M.; Chateigner, D.; Gil, O. Role of brucite dissolution in calcium carbonate precipitation from artificial and natural seawaters. *Cryst. Growth Des.* **2017**, *17*, 1502–1513. [[CrossRef](#)]
23. Bano, M.; Rodger, M.; Quigley, D. New Insight into the Stability of CaCO₃ Surfaces and Nanoparticles via Molecular Simulation. *Langmuir* **2014**, *30*, 7513–7521. [[CrossRef](#)]
24. Vuong, P.; McKinley, A.; Kaur, P. Understanding biofouling and contaminant accretion on submerged marine structures. *npj Mater. Degrad.* **2023**, *50*, 1–11. [[CrossRef](#)]
25. Nataly, C.; Shiladitya, P. The Effect of Temperature and Local pH on Calcareous Deposit Formation in Damaged Thermal Spray Aluminum (TSA) Coatings and Its Implication on Corrosion Mitigation of Offshore Steel Structures. *Coatings* **2017**, *7*, 52. [[CrossRef](#)]
26. Li, C.; Du, M.; Qiu, J.; Zhang, J.; Gao, C. Influence of Temperature on the Protectiveness and Morphological Characteristics of Calcareous Deposits Polarized by Galvanostatic Mode. *Acta Metall. Sin.* **2014**, *27*, 131–139. [[CrossRef](#)]
27. Chi, N.V.; Quan, L.H.; Linh, C.N.; Quang, N.Q.; Anh, N.D.; Kien, D.V.; Hoa, N.V. Electrodeposition of Cu-Reinforced Polyaniline Coating for Protection of AH36 Steel in Natural Seawater. *Coatings* **2022**, *12*, 1680. [[CrossRef](#)]
28. Nguyen, V.C.; Cao, N.L.; Dong, V.K.; Le, H.Q.; Mai, V.M.; Nong, Q.Q.; Zyablov, A.N. Corrosion behavior of AH-36 steel in seawater. *Butlerov Commun.* **2020**, *63*, 113–118. [[CrossRef](#)]
29. Nguyen, V.C.; Cao, N.L.; Dong, V.K.; Le, H.Q.; Nong, Q.Q.; Zyablov, A.N. Study on structural steel AH-36 corrosion in the marine environment of Vietnam. *ChemChemTech* **2021**, *64*, 139–144. [[CrossRef](#)]
30. Li, C.J.; Du, M. The growth mechanism of calcareous deposits under various hydrostatic pressures during the cathodic protection of carbon steel in seawater. *RSC Adv.* **2017**, *7*, 28819–28825. [[CrossRef](#)]
31. Belmonte, M.R.; Quiroz, T.P.; Salas, B.V.; Madrid, M.M.; Acosta, A.T.; Calderon, J.P.; Wiener, M.S. Characterization of steel surface under cathodic protection in seawater. *Anti-Corros. Methods Mater.* **2013**, *60*, 160–167. [[CrossRef](#)]

Disclaimer/Publisher’s Note: The statements, opinions and data contained in all publications are solely those of the individual author(s) and contributor(s) and not of MDPI and/or the editor(s). MDPI and/or the editor(s) disclaim responsibility for any injury to people or property resulting from any ideas, methods, instructions or products referred to in the content.